The surface abundances of red supergiants at core collapse

Ben Davies, Luc Dessart

Monthly Notices
of the
ROYAL ASTRONOMICAL SOCIETY

MNRAS **483,** 887–895 (2019)
Advance Access publication 2018 November 19

doi:10.1093/mnras/sty3138

The surface abundances of red supergiants at core collapse

Ben Davies[1]★ and Luc Dessart[2]

[1]*Astrophysics Research Institute, Liverpool John Moores University, Liverpool Science Park ic2, 146 Brownlow Hill, Liverpool L3 5RF, UK*
[2]*Unidad Mixta Internacional Franco-Chilena de Astronomía (CNRS, UMI 3386), Departamento de Astronomía, Universidad de Chile, Camino El Observatorio 1515, Las Condes, Santiago, Chile*

Accepted 2018 November 12. Received 2018 November 9; in original form 2018 July 10

ABSTRACT

In the first weeks-to-months of a Type II-P supernova (SN), the spectrum formation region is within the hydrogen-rich envelope of the exploding star. Optical spectra taken within a few days of the SN explosion, when the photosphere is hot, show features of ionized carbon, nitrogen, and oxygen, as well as hydrogen and helium. Quantitative analysis of this very early phase may therefore constrain the chemical abundances of the stellar envelope at the point of core collapse. Using existing and new evolutionary calculations for red supergiants (RSGs), we show that the predictions for the terminal surface [C/N] ratio is correlated with the initial mass of the progenitor star. Specifically, a star with an initial mass above 20 $M_\odot$ exploding in the RSG phase should have an unequivocal signal of a low [C/N] abundance. Furthermore, we show that the model predictions are relatively insensitive to uncertainties in the treatment of convective mixing. Although there is a dependence on initial rotation, this can be dealt with in a probabilistic sense by convolving the model predictions with the observed distribution of stellar rotation rates. Using numerical experiments, we present a strategy for using very early-time spectroscopy to determine the upper limit to the progenitor mass distribution for Type II-P SNe.

Key words: stars: abundances – stars: evolution – stars: massive – supergiants – supernovae: general.

1 INTRODUCTION

Pre-explosion imaging of the sites of nearby core-collapse supernovae (SNe) has provided unequivocal evidence for the progenitors of hydrogen-rich 'plateau' (Type II-P) SNe being red supergiants (RSGs; Smartt et al. 2004, 2009). From these data it is then possible to make quantitative comparisons between the properties of the exploding star and the predictions made by stellar evolution models about the terminal properties of massive stars.

One such test is to determine the initial masses $M_{\rm init}$ of a sample of II-P progenitors and compare the observed mass range to model predictions. Early results suggested that perhaps the upper mass limit for II-P progenitors was substantially lower than expected, $\sim$17 $M_\odot$ as opposed to the $\gtrsim$25 $M_\odot$ predicted by models (Smartt et al. 2009; Smartt 2015). However, this result has since been challenged by Davies & Beasor (2018), who argued that systematic errors in the conversion of pre-explosion brightness to initial mass, combined with a small sample size, reduce the statistical significance of this result to well below 3σ.

Other authors have attempted to infer the mass of the progenitor by studying the SN radiation (e.g. Bersten, Benvenuto & Hamuy 2011; Dessart et al. 2013; Utrobin & Chugai 2017). Modelling of the light curve and photospheric properties during the plateau phase can yield an estimate of the mass of the H-rich envelope at the point of explosion, though assumptions about the He-core mass and the mass-loss history are required to then obtain $M_{\rm init}$. Further, modelling the SN spectrum during the nebular phase has provided estimates of the oxygen yield, which is a function of the progenitor mass (e.g. Jerkstrand et al. 2014; Valenti et al. 2016). However, as yet, there appears to be a lack of agreement between the hydro, nebular, and pre-explosion estimates for the progenitor initial masses (e.g. Davies & Beasor 2018).

In this paper, we present an independent method for inferring the progenitor mass of a II-P that utilizes the observed abundance ratios in the very early phases of the SN explosion. The surface composition of the progenitor star at core collapse should prevail throughout a substantial fraction of the H-rich envelope, depending on how mixed it becomes during the explosion. Here, we have chosen to focus on the spectral appearance at very early times of less than a couple of days. The reason for this is twofold: first, at these early times, the spectral formation region is hot (several $\times$ 10^4 K), and so the spectra are dominated by high-ionization species such as C III–IV, N III–IV, and O V (Dessart, John Hillier & Audit 2017; Yaron et al. 2017). From these spectral lines it is possible to estimate the pre-explosion carbon, nitrogen, and oxygen (CNO) abundances,

★ E-mail: b.davies@ljmu.ac.uk

which as we will show are sensitive to the initial mass of the SN progenitor. Secondly, at such early times we can be confident that explosive mixing has not yet modified the abundances within the spectrum formation region of the supernova.

In Section 2, we describe how the surface abundances are modified during a star's evolution, and how it depends on the initial mass of the star. In Section 3, we show the effect of these abundances on the early spectra. In Section 4, we discuss the prospects for using early-time spectra to determine progenitor masses. We conclude in Section 5.

2 EVOLUTIONARY MODELS

In this section, we introduce the chemical signatures of a massive progenitor that can be seen in SN spectra. These signatures relate to the abundances of CNO. Broadly, core hydrogen burning during the main sequence (MS) alters the relative CNO mix in the centre of the star. As a result of the convective mixing in the centre of the star, while on the MS, and the dredge-up by the surface and intermediate convective zones (ICZs) as the star becomes a RSG, this polluted material is brought to the surface.

To demonstrate this effect and study its causes, we study two sets of evolutionary models, both computed at solar metallicity. The first we use are the densely sampled mass tracks created using the MESAcode (Paxton et al. 2011, 2013, 2015) published by Choi et al. (2016, hereafter the MIST models). We compare the results of these models to a second set of models, those published by Ekström et al. (2012, hereafter E12) using the Geneva evolutionary code. Both of these works study non-rotating and fast-rotating (40 per cent of breakup) stars, employ similar prescriptions for mass loss $\dot{M}$ on the MS and cool supergiant phases,[1] and evolve the stars to the point of carbon depletion in the core. However, there are key differences in the way the two suites of models treat convection and interior mixing. Our reason for choosing particularly these two sets of models is to study the robustness of their predictions to the details of convection.

The approach of the E12 models is to adopt the Schwarzschild criterion for convective instability. The energy transport in the convective zones is dealt with using mixing length theory (MLT), with a mixing length parameter of $\alpha = 1.6$. Convective overshooting from the core is implemented by extending the mixing boundary beyond the edge of the convective core by 0.1 times the local pressure scale height. Since the Ledoux criterion is not used, there is no semiconvection in the E12 models.

In the MIST models, convective energy transport is again treated using MLT with $\alpha = 1.82$. However, this time the criterion for convective instability comes from Ledoux, which adds in the stabilizing effect of any composition gradient. Regions that are Schwarzschild unstable but Ledoux stable are mixed according to a semiconvection parameter of $\alpha_{\rm semi} = 0.1$. Another difference from E12 is the treatment of core overshooting – this time, the diffusion coefficient falls off exponentially from the edge of the core with a characteristic length-scale of 0.016 times the local pressure scale height. One further difference to the E12 is that MIST adopts overshoot at the base of the intermediate and surface convective layers (sometimes referred to as 'undershoot'), as well as at the top. Both overshoot on both edges of the convective shells are characterized with $\alpha_{\rm os} = 0.0174$.

[1]Subtle differences in the $\dot{M}$ implementation will be discussed later.

In the following sections, we use these two suites of models with contrasting treatment of internal mixing to first demonstrate the trend of surface CNO abundances with initial mass, to explain the underlying causes of this effect, and its dependence on the details of internal mixing.

2.1 Evolution across the H–R diagram

Before we look at the trends of surface properties with increasing initial mass, we first look in detail at what happens in a star as it crosses the H–R diagram to the RSG phase. We do this in order to understand how and when dredge-up takes place, since it is this event that is primarily responsible for the surface abundances at the end of the RSG phase.

Once a star of initial mass $\sim$10 $M_\odot$ leaves the MS, it will cross the H–R diagram very rapidly on a time-scale comparable to the thermal time-scale of the core. Higher mass stars, however, cross the H–R diagram more slowly. The initial mass at which this change in evolutionary time-scale first occurs can be inferred from the morphology of the evolutionary track. In the case of rapid redward evolution of the star, the expansion is primarily adiabatic, and the star's luminosity L decreases during this phase. In contrast, slower redward evolution is quasi-hydrostatic, and tends to occur at almost constant L. For almost all major contemporary single-star evolutionary tracks, the transition from rapid (decreasing L) to slow ($\sim$constant L) crossing of the yellow void is seen to occur somewhere between 15 and 20 $M_\odot$.

There are two factors that affect the crossing of the H–R diagram. These are the point of core He ignition, and the location of the ICZ with respect to the hydrogen-burning shell. Below we explore each of these factors in more detail. To do this, we have taken the MIST 'inlist' files from the MIST models and recomputed the evolution[2] of selected models to obtain the internal profiles as a function of time. For details on these models, including the choices made with regard to mass resolution and time steps, we refer the reader to the MIST models (see also Farmer et al. 2016).

2.1.1 *The intermediate convective zone*

The main factor affecting how a star crosses the H–R diagram is the development of an intermediate convective zone (ICZ) at the end of the MS, above the convective core but well below the surface of the star. The details of the behaviour of the ICZ are explored in Figs 2 and 3. In the first of these figures, we present Kippenhahn diagrams of three different stages in the evolution of non-rotating 12 $M_\odot$ star. In the left-hand panel, we see a convective core (black cross-hatched region) that gradually contracts in mass throughout the MS. The centre panel shows the end of the MS, where the end of core H-burning coincides with the formation of the ICZ and the H-burning shell (denoted by the white cross-hatched region), which in this model do not strongly overlap. This contrasts with the 25 $M_\odot$ non-rotating model (centre panel of Fig. 3), where there is a large degree of overlap between the H-burning shell and the ICZ. These two features first overlap at around 16 $M_\odot$, and are well separated at lower masses. The overlap ensures that fresh H is continually provided to the shell, increasing the energy generation rate, and helps to slow the evolution across the H–R diagram in the time between core H exhaustion and core He ignition.

[2]Our calculations were performed using MESA v7503, following the MIST models.

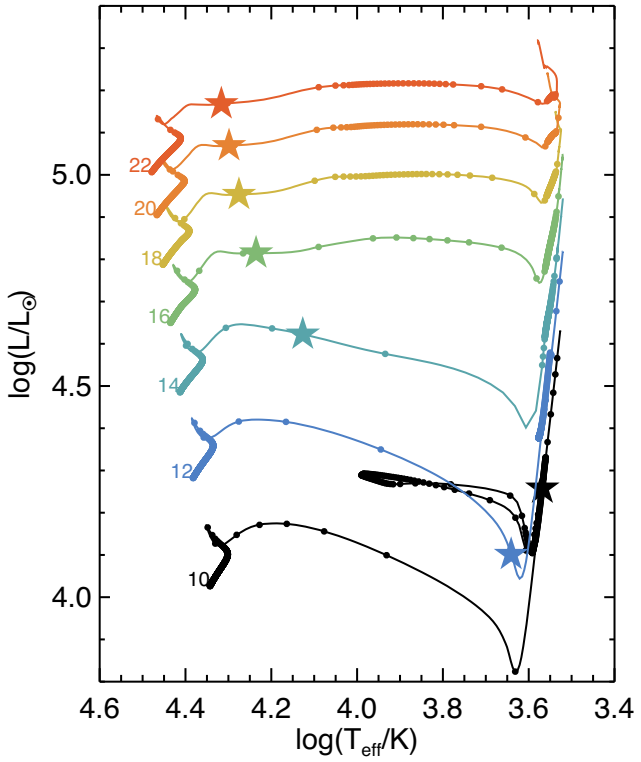

Figure 1. Evolutionary tracks of the non-rotating MIST models from midway through the main-sequence to core carbon depletion (cCd). The stars indicate the point of core He ignition. The filled circles are the evolutionary tracks resampled onto an evenly spaced time axis with spacing 5000 yr, to illustrate how long the stars spend in each phase.

The depth in the star at which the ICZ forms after leaving the MS is perhaps the evolutionary aspect most sensitive to the treatment of convection. This was discussed by Georgy, Saio & Meynet (2014), who experimented with switching between Ledoux and Schwarzschild criteria, and found that the stabilizing effect of the composition gradient lifted the ICZ to higher layers of the star in the Ledoux model compared to the Schwarzschild model. In E12, the default is to use Schwarzschild, whereas in MIST the Ledoux criterion is employed with a semiconvection coefficient of $\alpha_{\rm semi} = 0.1$. The important property of the ICZ in terms of the evolution of the star is whether or not it overlaps the H-burning shell, and this is more likely at higher initial stellar masses.

2.1.2 *The evolution of surface abundances*

In Figs 2 and 3, the colour scale represents the [C/N] ratio: red represents unpolluted material with the star's initial relative abundances and blue indicates zones heavily polluted by the products of CNO processing. The left-hand panel focuses on the beginning of the MS. The polluted zone (the region colour coded as blue in Fig. 2) of the 12 M⊙ model initially coincides with the boundary of the convective core at $M_{\rm r} \simeq 4.5$ M⊙. By the end of the MS (centre panel), the core convective zone shrinks in mass to $M_{\rm r} \simeq 4$ M⊙, but the polluted zone moves outwards to $M_{\rm r} \simeq 6$ M⊙. The latter effect is caused by the C abundance in the radiative zone being higher than that in the outer convective core, meaning that CNO burning at the bottom of the radiative zone can dominate that at the edge of the convective core. Whilst relatively little energy is generated by this burning at the base of the radiative zone, it can still substantially modify the relative CNO abundances.

After the 12 M⊙ star has left the MS, it rapidly crosses the H–R diagram and becomes an RSG. At this point the star develops an outer convection zone that reaches from the surface down to the inner 4 M⊙ that dredges up material from deep within the polluted zone. This results in a rapid decrease in the surface [C/N], illustrated by the change in plotting colour of the envelope. During the later stages of nuclear burning the surface convective zone may deepen, further decreasing the surface [C/N].

The same qualitative behaviour is seen in the 25 M⊙ model as in the 12 M⊙ model. However, the terminal abundances in the envelope are clearly different, with the more massive star having a lower [C/N] ratio. This is caused primarily by the larger convective core as a fraction of the total mass of the star at zero-age main sequence (ZAMS): the larger the core, the greater the reservoir of polluted material available to be dredged-up at the RSG phase. In the centre panels of Figs 2 and 3, we see that the interior polluted zone (coloured blue) of the 12 M⊙ star reaches the inner 6 M⊙ (50 per cent of the star by mass), whereas in the 25 M⊙ star it's

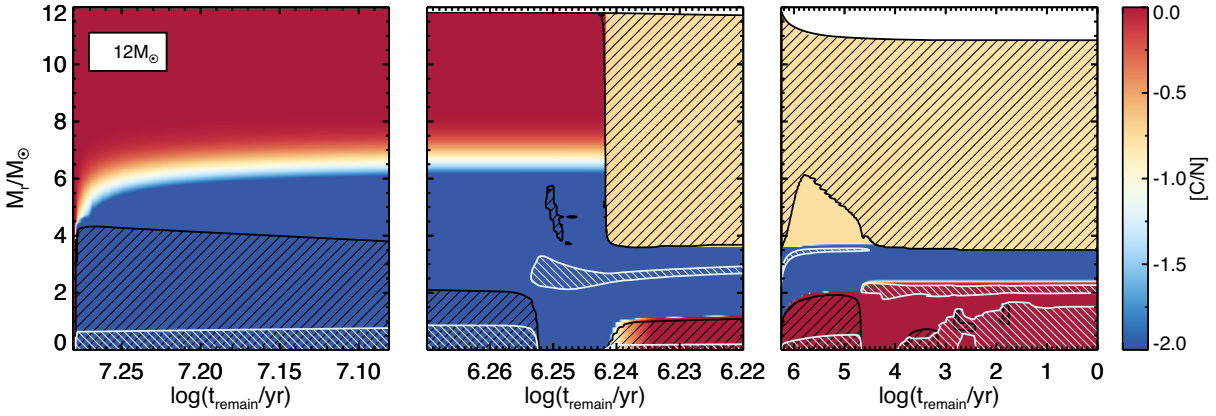

Figure 2. Kippenhahn diagram for the MIST 12 $M_\odot$ non-rotating model with standard cool star mass loss. The colour scale shows the C/N ratio relative to solar, the black cross-hatch areas show the regions of strong convection, and the white cross-hatch areas show the regions of strong nuclear burning. The three panels show the main-sequence evolution, a zoom of the end of core H-burning and beginning of core He-burning, and from core He burning to core C depletion.

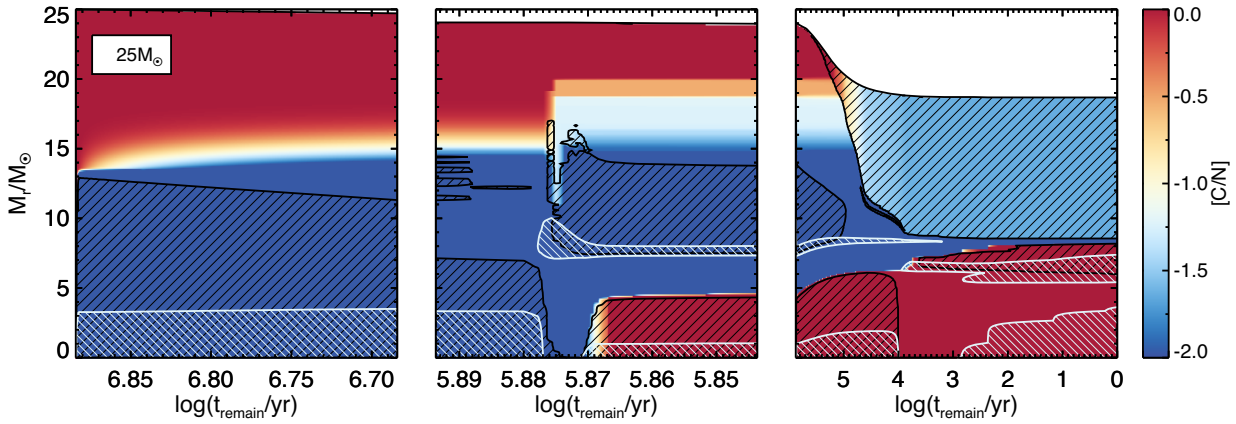

Figure 3. Same as Fig. 2 but for the 25 $M_{\odot}$ MIST model with no rotation and standard mass loss.

the inner 15 M⊙ (60 per cent). This trend of decreasing [C/N] as a function of increasing initial mass is studied further in Section 2.2.

2.1.3 The effect of mass loss on surface abundances

One further factor that can affect the surface abundances after dredge-up is mass loss. Specifically, if a large amount of the envelope has been lost *prior* to dredge-up, then the mass of the unpolluted material to be mixed in with the polluted material is decreased, resulting in a lower [C/N] ratio post dredge-up. During the MS, the fraction of mass lost by the star is negligible for those initial masses studied here ($\lesssim$1 M⊙). However, an erroneous result can occur if the star crosses the H–R diagram at a slower pace such that it experiences a prolonged yellow supergiant (YSG) phase prior to dredge-up, which we now describe.

In most evolutionary codes, mass-loss rates $\dot{M}$ are implemented using analytical formulae that relate $\dot{M}$ to the star's luminosity, temperature, and metallicity. Once the star evolved to temperatures below ∼10 kK, the mass-loss 'prescription' is switched to that of de Jager, Nieuwenhuijzen & van der Hucht (1988). This prescription is a functional fit to empirically derived mass-loss rates from various studies in the 1970s/1980s for a sample of stars spanning spectral types from O to M. The shortcomings of this prescription during the RSG phase have been pointed out by Beasor & Davies (2018), but its description of mass loss during the YSG phase is perhaps even more uncertain. Here, the de Jager et al. (1988) mass-loss rates are based on only seven stars, many of which are well-known extreme objects such as IRC+10420. Further, the individual $\dot{M}$ measurements are dubious, and the dispersion of the individual stars about the best-fitting relation is as large as ±0.7 dex.

Nevertheless, the de Jager et al. (1988) prescription is adopted almost universally by evolutionary codes for massive cool stars. Should a model star experience a prolonged YSG phase, the large $\dot{M}$ assigned to the star by the de Jager et al. (1988) prescription causes a large amount of envelope to be lost prior to dredge-up. As will be discussed in Section 2.2, this can result in anomalously low terminal [C/N] ratios for these stars.

2.2 The trend of [C/N] with initial stellar mass

In Fig. 4, we plot the surface C/N ratio relative to solar at the onset of core carbon depletion (cCd) as a function of initial stellar mass $M_{\rm init}$ for the MIST and E12 models, both non-rotating and rotating.

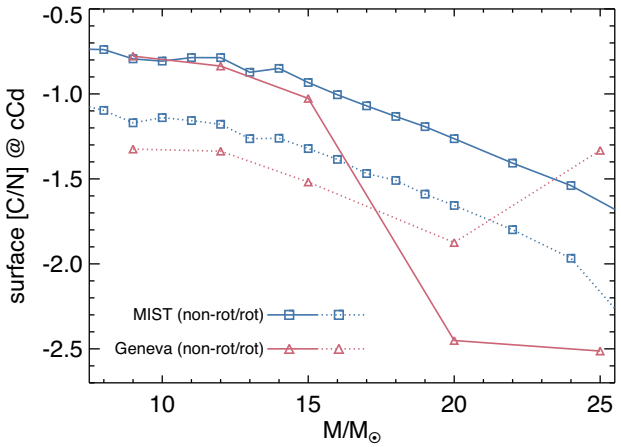

Figure 4. The surface ratio of C/N relative to the initial value at the onset of core carbon depletion (cCd) as a function of the star's initial mass, according to the MIST and Geneva (E12) models. Solid lines are non-rotating, dotted lines are rotating at 40 per cent critical.

the MIST models, which were computed on a much denser grid than the E12 models, display a clear and monotonic trend of decreasing [C/N] for stars of increasing $M_{\rm init}$. As argued in the previous section, the cause of this trend is primarily the larger convective cores of massive stars at ZAMS as a fraction of their total mass, which results in a larger (by mass) reservoir of polluted material above the core at the end of the MS. This polluted material is then mixed-in to the convective envelope during the RSG phase.

Also plotted in Fig. 4 are the MIST rotating models. Increased internal mixing in the rotating stars produces a trend that is qualitatively similar to that of the non-rotating models, but is offset to lower [C/N] by around 0.3–0.4 dex. This offset is caused by the combination of a larger core, and enhanced internal mixing during the MS that allows the products of nuclear burning in the core to diffuse outwards to the intermediate layers where it can be dredged-up during the RSG phase. Since the two values of initial rotation present in the MIST models (0 and 40 per cent of breakup) are somewhat extreme values, we expect a typical star to lie somewhere in between these two values. This then demonstrates that the likely systematic error in [C/N] due to rotation is around ±0.15–0.2 dex. This is discussed in greater detail in Section 4.

In terms of the E12 non-rotating/rotating models (plotted in Fig. 4 as blue lines), we can see that up to 15 M⊙ the two non-rotating tracks produce almost exactly the same behaviour. The rotating E12 models are more depleted in [C/N] by ∼0.15 dex compared to MIST, due to the different way rotational mixing is treated, but qualitatively the same trend is seen. At 20 M⊙ and above, the E12 and MIST results diverge. This is *not* caused by the treatment of mixing. In E12, the mass-loss scaling in the RSG phase ($T_{\rm eff} < 5$ kK) has been enhanced by a factor of 3 compared to that in MIST, which contemporary observations suggest is not well justified.[3] This threefold increase in the mass-loss rate, coupled with the much slower rate at which the star crosses the H–R diagram and the high values of $\dot{M}$ assigned to YSGs/RSGs by the de Jager et al. (1988) prescription, means that a substantial fraction of the stellar envelope can be lost before the star has reached its minimum $T_{\rm eff}$ (see Section 2.1.2). Hence, by the time the convective envelope reaches deepest into the star, its mass is greatly reduced compared to a model with the standard mass-loss rate prescription. This causes the ratio of polluted to pristine material to be larger, and the surface [C/N] to be lower.

2.3 Sensitivity to free parameters relating to convection

The similarity of the E12 and MIST models up to 15 M⊙ hints that the treatment of convection is not so important with regard to the terminal surface abundances (see also Martins & Palacios 2013). To perform a more detailed check of this we have computed new models at 15, 20, and 25 M⊙, in which we have altered how convection is treated. In addition to the fiducial non-rotating MIST models, we have computed further families of models in which the set-up is the same as MIST but for one change.[4]

(i) The mixing length parameter is increased to $\alpha_{\rm MLT} = 3.0$. The fiducial value is calibrated against the Sun, however, there is no reason to expect that this same value should be employed for all stars of all masses. Increasing the value of $\alpha_{\rm MLT}$ is motivated by the observational evidence that RSGs may have higher $T_{\rm eff}$ than in current evolutionary models (Davies et al. 2013; Tabernero et al. 2018), and that the early colour evolution of SNe II-P require the progenitor RSG to be more compact than for a mixing length characterized by $\alpha_{\rm MLT} = 1.6$ (Dessart et al. 2013). The precise value of $\alpha_{\rm MLT} = 3.0$ used here is that tuned by Dessart et al. to fit the multiband light curve of SN 1999em. Latterly, Chun et al. (2018) attempted to tune $\alpha_{\rm MLT}$ by fitting the observed effective temperatures of RSG, finding values of $2.0 < \alpha_{\rm MLT} < 2.5$. In this subset of models, the adopted $\alpha_{\rm MLT} = 3.0$ is an extreme limit, which allows us to study the maximal possible effect of this free parameter.

(ii) Following the E12 models, we have switched off semiconvection and the Ledoux criterion. These models are referred to as the Schwarzschild models.

(iii) In the opposite extreme to the above models, we have computed models that are purely Ledoux (i.e. no semiconvection).

(iv) Finally, we have computed two further sets of models in which we have deactivated overshoot at the base of the convective regions (also known as 'undershoot'). In the first of these, we deactivate undershoot at the base of the envelope, which we call 'no-und-env'. In the second, we deactivate undershoot entirely that is no undershoot in the envelope or in any of the intermediate shells (called 'no-und-all').

In Fig. 5, we plot the evolutionary tracks and the surface abundances as a function of time for the several families of models (fiducial ≡ MIST, $\alpha_{\rm MLT} = 3$, Schwarzschild, Ledoux, and the no undershoot models). In terms of their paths on the H–R diagram, most of the models are very similar. The $\alpha_{\rm MLT} = 3$ models have slightly higher $T_{\rm eff}$ on the RSG branch, which is expected. A less obvious result is seen in the 15 and 20 M⊙ models with all forms of undershoot deactivated ('no-und-all'). In these models, the lack of undershoot in the ICZ at the end of the MS results in a smaller ICZ, causing less overlap with the H-burning shell. Therefore, these models cross the H–R diagram on a thermal time-scale, causing the luminosity to drop as they do so, before rapidly rising again once they arrive on the RSG branch (see Section 2.1).

The pace at which the stars evolve once leaving the MS, and hence the rate at which the surface abundances are polluted, is slightly different in each family of model (right-hand panel of Fig. 5). In the majority of models, the asymptotic [C/N] value at each of the three masses is almost indistinguishable regardless of how convection is treated. The exceptions are discussed below.

(i) In the 'no-und-all' models, all masses have lower terminal [C/N] by between 0.2 and 0.4 dex. This is caused by more rapid dredge-up at the end of the MS (in the 15 and 20 M⊙ models), as well as the smaller ICZ reducing the amount of material mixed from deep in the star to the intermediate zones, from where it is dredged to the surface in the RSG phase.

(ii) The Schwarzschild model evolves to a slightly lower (−0.3 dex) [C/N], however, this is caused by a prolonged YSG phase, which we have argued here is somewhat spurious. Without the stabilizing effect of the μ-gradient term, the ICZ at the end of the MS forms at deeper layers in the star with respect to the fiducial model. This has the effect of stalling the star's traversal of the H–R diagram, holding it in the yellow, and subjecting it to a high mass-loss rate (see Section 2.1.2). This causes a substantial portion of the envelope to be lost prior to dredge-up, and ultimately in the terminal [C/N] being lower. This is similar to what happens to the 20 M⊙ model in E12 (see Section 2).

From these tests, we conclude that the degree of mixing as a function of evolutionary phase is somewhat sensitive to how convection is implemented.[5] However, by the time the core is depleted of C (within $\sim 10^3$ yr of SN), the majority of our variant models have surface [C/N] ratios consistent to within less than 0.1 dex at a given

[3]The physical justification in E12 for increasing the mass-loss rates in the cool supergiant phase is that, at masses of 20 M⊙ and higher, the star may exceed the classical Eddington limit in their envelope at some point in their post-MS evolution. It is argued that one might expect this to cause $\dot{M}$ to increase. The choice of an enhancement factor of 3 was chosen to mimic the highest $\dot{M}$ RSGs. However, recent studies of RSG mass loss have claimed that total mass lost integrated over the RSG lifetime may be substantially lower than that in models that apply the standard (e.g. de Jager et al. 1988) mass-loss prescriptions (Beasor & Davies 2018).

[4]An effect we do not explore here is that of altering the core overshooting parameter. As pointed out by Meynet & Maeder (2000), the effects of rotation and core overshoot are largely degenerate, since both serve to mix the outer core with the inner envelope. Since the effects of rotation are studied here, we do not explore the effects of altering core overshoot explicitly.

[5]A caveat to our analysis here is that any change that substantially alters the evolution of the star, such as turning off undershooting, would likely require the other model free parameters (e.g. mixing length and overshooting) to be recalibrated to retain the agreement with observations. The effect this would have on the systematic errors on [C/N] is not known.

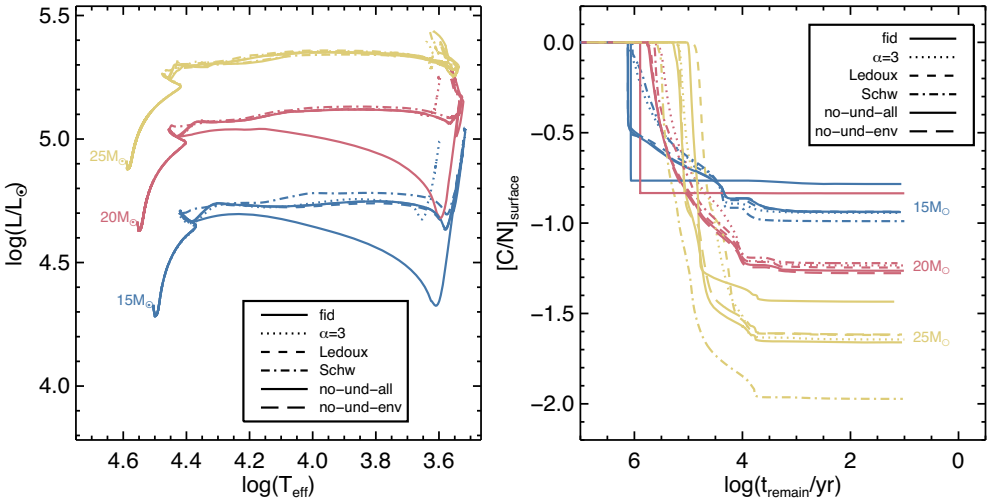

Figure 5. The dependence of stellar evolution on the treatment of convection. Left: H–R diagram. Right: surface [C/N] as a function of time. See text for details on the families of models.

initial mass. The biggest sensitivity is seen when we completely deactivate all forms of undershooting, which shifts the terminal [C/N] higher by 0.2–0.4 dex, though the same qualitative trend of [C/N] with initial mass is still seen. At the very worst, our variant models have a difference in terminal [C/N] of ±0.25 dex (i.e. the difference between the 25 M⊙ 'Schwarzschild' and 'no-und-all' models). A more important source of systematic uncertainty is stellar rotation, which we discuss further in Section 4.

3 EXPECTATIONS FOR SN SPECTRA

In the preceding sections, we have demonstrated that there should be a clear trend of decreasing [C/N] with increasing MS mass at the surface of RSG stars. This trend should persist until core collapse and the successful explosion of the star as a Type II SN. In this section, we discuss how CNO abundances may be constrained from Type II SN spectra.

Quantitative spectroscopy of Type II SNe is a very complicated task because of a number of different challenges. The large SN expansion rate produces broad Doppler-broadened line profiles that often suffer from line overlap. This broadening also smears the line flux in velocity (of wavelength) space. It can prevent the clear identification of a given transition or its flux contribution to the line blend. Furthermore, Type II SNe are usually discovered a few days after explosion, at a time when the photosphere has cooled to about 10 000 K. At that time and beyond, the spectrum tends to show lines of H I and He I, with only a few lines of CNO elements (typically O I 7774 Å, which overlaps with a broad atmospheric absorption for SNe at low redshifts; C I lines in the red part of the spectrum). For SN 1999em, SN 1999gi, SN 2005cs, or SN 2006bp, lines of He II, O II, or N II were seen as weak features and for a short while (Dessart & Hillier 2005; Baron, Branch & Hauschildt 2007; Quimby et al. 2007; Dessart et al. 2008). Abundance determinations require detailed non-local thermodynamic equilibrium (LTE) radiative transfer modelling. For example, not accounting for departures from LTE poses severe problems with the determination of the He abundance in early-time spectra (compare the results from Eastman & Kirshner 1989 with those of Dessart & Hillier 2010). Time dependence in the non-LTE rate equations is also essential for accurate abundance determinations because this time dependence impacts the ionization of all species (Utrobin & Chugai 2005; Dessart & Hillier 2008). Even with all the necessary physics, the sensitivity of line strengths to abundance changes is weak (see e.g. Dessart & Hillier 2006).

Here we exploit the possibility that early-time spectra may be obtained for Type II SN with the advent of high-cadence surveys combined with prompt spectroscopic follow-up. In this case, SNe may be more routinely caught when their photosphere is much hotter, exhibiting lines from ionized He and CNO elements. In addition, if the environment of the RSG progenitor is engulfed in a substantial amount of material, these lines will be electron-scattering broadened (rather than Doppler broadened). Because there is no blueshift of the line profile, the peak flux occurs at the rest wavelength and the line identification is facilitated. Several SNe have revealed narrow line profiles of ionized He and CNO from a few hours to a few days after discovery, for example, SN 1998S (Chugai 2001; Fassia et al. 2001; Shivvers et al. 2015; Dessart et al. 2016), SN 2013cu (Gal-Yam et al. 2014; Groh 2014; Gräfener & Vink 2016), or SN 2013fs (Yaron et al. 2017).

For SN 2013fs, the spectra first exhibit lines of O V– VI and He II. As the photospheric temperature drops, the ionization decreases and spectral lines of O IV and N V appear, followed after a few days by a dominance of He I and H I. The rich spectrum in CNO lines during the first hours to days thus turns into one that contains mostly lines of H I and He I, which are largely insensitive to the nuclear evolution in the progenitor star.

Using non-LTE radiative transfer and radiation hydrodynamic simulations, Dessart et al. (2017) showed that the early-time spectra of SN 2013fs can be qualitatively reproduced with a fiducial RSG surface composition. Here, we present new simulations for their model r1w5r (performed in the same manner as described in Dessart et al. 2017) but this time we adopt the composition given by the surface chemistry of the 15, 20, and 25 $M_{\odot}$ models computed with MESA and described in the preceding section. Specifically, we use He, C, N, and O mass fractions listed in Table 1.

Fig. 6 shows the resulting spectra in three different spectral windows at 3.1, 12, and 24 h after shock breakout. The lines predicted in the model, which are also present in the observations of SN 2013fs (Yaron et al. 2017), are due to H I 4340, 4862, 6562 Å, He I 5875, 6678 Å, He II 4686, 4860, 5411, 6562 Å, C IV 5801–5812, 7110 Å,

Table 1. Mass fractions of He, C, N, and O used in the three models computed here.

$M_{\rm init}$	X(He)	X(C)	X(N) ($\times 10^{-3}$)	X(O)
15	0.344	1.29	3.3	4.7
20	0.410	0.87	4.7	3.7
25	0.474	0.48	6.5	2.2

N IV 4057, 7122 Å, N V 4610 Å, O V 5597 Å, and O VI 3811–3834 Å. In addition, there are strong abundance diagnostics in the near-infrared, with complexes of C III–IV in the *J* band and N V in the *H* band. One can clearly see the greater strength of N lines in the higher mass models, and the greater strength of C and O lines in the lower mass models. In particular, the [C/N] ratio is most discernable from the *J*- and *H*-band complexes at 12 h, and in the ratio of C IV 5801–5812 Å to N IV 7122 Å at 24 h. In practice, extracting a similar information on CNO abundances from observations will require a set of SNe at early times, so that one can identify a trend in line strengths for similar ionization/temperature conditions in the spectrum formation region.

Finally, we note that analysis of the spectrum of SN 2013cu taken at 15.5 h after explosion (Gal-Yam et al. 2014; Groh 2014; Gräfener & Vink 2016) reveals a similarly low [C/N] ratio as that predicted here for massive RSGs. This SN however was a Type IIb with a very low H-mass fraction, and had likely lost almost all of its H-rich envelope before exploding. Hence, the abundances seen in the early-time spectrum SN 2013cu likely reflect those at the base of the progenitor's H-rich envelope. To lose the entire envelope before exploding would require a very high mass-loss rate that is unlikely to be achieved merely by the wind of a single star (Beasor & Davies 2018), and is more likely indicative of mass transfer onto a binary companion. Since binary interaction greatly complicates stellar evolution, the correlation between terminal surface abundances and initial mass would almost certainly be lost. If a substantial H-rich envelope was intact at the point of core collapse, it would reveal itself as a prolonged 'plateau' (or high-brightness) phase in the SN light curve, and would indicate that no significant binary interaction had taken place. Therefore, a II-P light curve combined with a low [C/N] determined from early-time spectroscopy would together indicate a high-mass progenitor.

4 PROSPECTS

Having shown above that the mass dependence of the RSG surface abundances should be visible in early-time spectra, we now study the prospects of using these observational signatures to determine the mass function of SN II-P progenitors. We do this by simulating the predicted cumulative distribution of [C/N] ratios for a finite sample of SNe, factoring in both model and observation errors.

The first step is to define the predicted trend of terminal [C/N] with initial mass, accounting for the model uncertainties. As discussed in Section 2.3, by far the largest source of uncertainty is that of stellar rotation. Specifically, a model with an initial rotation speed of 40 per cent of breakup can have a final surface [C/N] ratio 0.4 dex lower than a non-rotating star. However, studies of stellar rotation have shown that the distribution of rotation speeds of massive stars is such that the majority have rotation rates halfway between these values (Ramírez-Agudelo et al. 2013). By taking the observed rotation rate distribution of Ramirez-Agudelo et al.,[6] and making the assumption that the trend of terminal surface [C/N] scales linearly with initial rotation speed,[7] we can make a probability density map for the [C/N] ratio as a function of initial mass. This is shown in Fig. 7, where the red, orange, and yellow contours illustrate where we expect 67, 95, and 99.7 per cent of stars to lie at a given initial mass.[8]

The next step is to simulate a population of massive stars by randomly sampling numbers from a Salpeter initial mass function (IMF) with an upper mass cut-off $M_{\rm max}$, which we leave as a free parameter. We then use Fig. 7 to randomly assign each star a terminal [C/N] ratio based on the probability distribution shown in this figure. Next, we factor in observational uncertainties by multiplying each star's terminal [C/N] by a Gaussian function centred on unity with a width $\sigma = 0.2$, to simulate an experimental uncertainty of ± 0.2 dex.[9] From these steps, we can then determine the expected distribution of [C/N] ratios for a given sample size and $M_{\rm max}$.

Finally, we take the simulated [C/N] distribution and attempt to recover the input value of $M_{\rm max}$. We do this by first determining the cumulative distribution of the simulated [C/N] ratios. We then compare this to a grid of similar distributions of the same sample size $\mathcal{N}$ but where $M_{\rm max}$ is allowed to vary. For a given trial, we measure the most likely $M_{\rm max}$ from a χ^2-minimization procedure. Since there are large stochastic effects, we repeat the measurement at each $M_{\rm max}$ and $\mathcal{N}$ 10^4 times, and determine the posterior probability distributions.

In Fig. 8, we show the results of this numerical experiment. The plot shows the difference between the input and output $M_{\rm max}$ and their 67 per cent probability limits as a function of sample size $\mathcal{N}$. There is a small systematic error in this type of analysis that causes one to underestimate the upper limit to a random distribution of numbers, since one cannot sample from numbers above this limit. However, it is possible to characterize and estimate this systematic error (see also Davies & Beasor 2018). The plot also shows that, for sample sizes greater than 50, the experimental errors on $M_{\rm max}$ begin to shrink to around ± 15 per cent. Though the current sample size of SNe with early-time spectroscopy is an order of magnitude smaller than this, the current collection rate of $\sim$4–5 yr^{-1} is already greater

[6] We note that the distribution of rotation rates in Ramírez-Agudelo et al. (2013) is that *observed* for MS O stars, rather than that at ZAMS.

[7] The knowledge of how terminal [C/N] scales with rotation speed at a fixed initial mass requires the computation of more models, which is beyond the scope of this work. Here, we make the simplest assumption of a linear scaling between the two.

[8] One major caveat to this experiment pertains to the model predictions of rotational mixing as a function of rotation rate. In both the MIST and E12 models, validation of the degree of rotational mixing is provided by comparing predictions of surface N abundances for MS massive stars with observations of OB stars. Agreement between the observations and the 'rotating' models is interpreted as a satisfactory calibration of the diffusion coefficients for rotational mixing. This is despite the fact that the 'rotating' models have rotation rates that are extreme in comparison to those typically observed. Since these diffusion coefficients are largely free parameters, in principle one could achieve a similar agreement between observed and predicted surface N abundances at lower rotation rates. Therefore, the absolute level of surface enrichment as a function of initial rotation rate may not be a robust model prediction.

[9] Though we do not yet know what the experimental uncertainties will be, ± 0.2 dex is a standard conservative error on abundance work in the modelling of hot star winds. The retrieval of abundances from early-time SN spectra, and degeneracies with other model parameters such as H/He and temperature, will be the subject of a future paper.

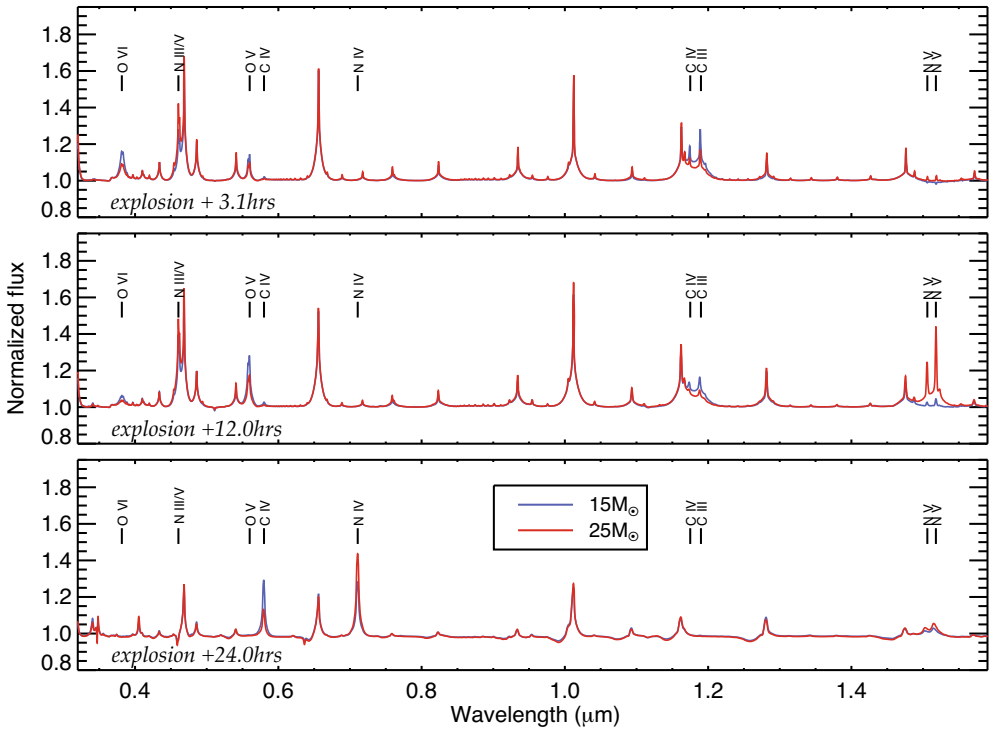

Figure 6. Variations in early-time spectra from the MIST non-rotating models at initial masses 15 and 25 M⊙. The three panels show the model spectra at the time in the bottom left of the plotting panel. Models were generated from the base model r1w5r from Dessart et al. (2017).

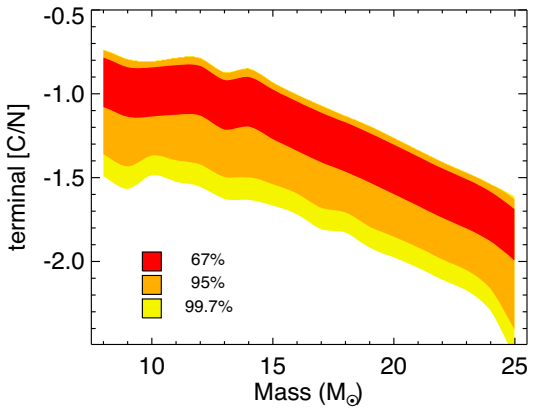

Figure 7. The probability distribution of terminal [C/N] ratios as a function of mass factoring in the observed distribution of rotation speeds of massive stars. The red, orange, and yellow contours encompass the 67, 95, and 99.7 per cent probability ranges (analogous to 1σ, 2σ, and 3σ).

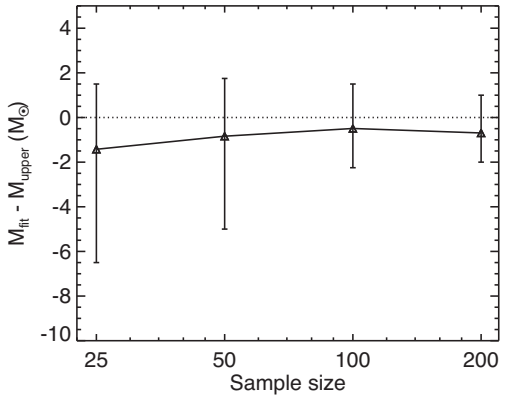

Figure 8. The accuracy and precision to which the upper mass limit $M_{\rm max}$ can be recovered from the terminal [C/N] ratios of a sample of SNe, as a function of sample size.

than that for SNe with pre-explosion imaging of the progenitors. Since this collection rate continues to grow, it is likely that a sample of ∼100 SNe with early-time spectra will be achieved within the next decade.

5 CONCLUSIONS

Using existing and new stellar evolution calculations, we have shown that the surface CNO abundances of RSGs at the end of their lives are correlated with their initial masses. Specifically, the ratio of carbon to nitrogen at the point of cCd [C/N], which is a diagnostic of how much nuclear processed material has been mixed into the envelope, is shown to decrease with increasing initial mass. We explored the sensitivity of this trend to how convection is treated using families of 'variant' models in which we alter semiconvection, mixing length, and undershooting. In the majority of cases the effect on [C/N] is less than ±0.1 dex, and is at worst ±0.25 dex. The dominant source of systematic error is the dependence on initial stellar rotation.

We have taken the end points of the evolution calculations and simulated how their SN spectra would look at very early times. Though subtle, there is a clear trend of increasing nitrogen and decreasing carbon line strengths at higher initial stellar masses. We argue that in principle this signature can be used to diagnose the initial mass of the SN progenitor.

Using a simple numerical experiment, we have set out an observing strategy to use the trend of terminal [C/N] with stellar mass to determine the upper limit to the mass range of SN II-P progenitors ($M_{\rm max}$). Assuming that [C/N] can be recovered to precision of $\pm$0.2 dex, and assuming that the initial rotation rate distribution of stars follows that of Galactic O stars, we show that $M_{\rm max}$ can be determined to within $\pm$3–4 M$\odot$ from a sample size of 50, and to within $\pm$2 M$\odot$ for a sample size of 100.

ACKNOWLEDGEMENTS

We thank the referee Cyril Georgy for the comments and suggestions that helped us improve the paper. For numerous constructive discussions we thank Dave Arnett, Emma Beasor, Sylvia Ekstrom, John Hillier, Raphael Hirschi, Georges Meynet, and Nathan Smith. This work made use of the IDL astronomy library, available at https://idlastro.gsfc.nasa.gov, and the Coyote IDL graphics library.

REFERENCES

Baron E., Branch D., Hauschildt P. H., 2007, ApJ, 662, 1148
Beasor E. R., Davies B., 2018, MNRAS, 475, 55
Bersten M. C., Benvenuto O., Hamuy M., 2011, ApJ, 729, 61
Choi J., Dotter A., Conroy C., Cantiello M., Paxton B., Johnson B. D., 2016, ApJ, 823, 10
Chun S.-H., Yoon S.-C., Jung M.-K., Kim D. U., Kim J., 2018, ApJ, 853, 79
Davies B., Beasor E. R., 2018, MNRAS, 474, 2116
Davies B. et al., 2013, ApJ, 767, 3
de Jager C., Nieuwenhuijzen H., van der Hucht K. A., 1988, A&AS, 72, 259
Dessart L., Hillier D. J., 2005, A&A, 437, 667
Dessart L., Hillier D. J., 2006, A&A, 447, 691
Dessart L., Hillier D. J., 2008, MNRAS, 383, 57
Dessart L., Hillier D. J., 2010, MNRAS, 405, 2141
Dessart L. et al., 2008, ApJ, 675, 644
Dessart L., Hillier D. J., Waldman R., Livne E., 2013, MNRAS, 433, 1745
Dessart L., Hillier D. J., Audit E., Livne E., Waldman R., 2016, MNRAS, 458, 2094
Dessart L., John Hillier D., Audit E., 2017, A&A, 605, A83
Eastman R. G., Kirshner R. P., 1989, ApJ, 347, 771
Ekström S. et al., 2012, A&A, 537, A146(E12)
Farmer R., Fields C. E., Petermann I., Dessart L., Cantiello M., Paxton B., Timmes F. X., 2016, ApJS, 227, 22
Fassia A. et al., 2001, MNRAS, 325, 907
Gal-Yam A. et al., 2014, Nature, 509, 471
Georgy C., Saio H., Meynet G., 2014, MNRAS, 439, L6
Gräfener G., Vink J. S., 2016, MNRAS, 455, 112
Groh J. H., 2014, A&A, 572, L11
Jerkstrand A., Smartt S. J., Fraser M., Fransson C., Sollerman J., Taddia F., Kotak R., 2014, MNRAS, 439, 3694
Martins F., Palacios A., 2013, A&A, 560, A16
Meynet G., Maeder A., 2000, A&A, 361, 101
Paxton B., Bildsten L., Dotter A., Herwig F., Lesaffre P., Timmes F., 2011, ApJS, 192, 3
Paxton B. et al., 2013, ApJS, 208, 4
Paxton B. et al., 2015, ApJS, 220, 15
Quimby R. M., Wheeler J. C., Höflich P., Akerlof C. W., Brown P. J., Rykoff E. S., 2007, ApJ, 666, 1093
Ramírez-Agudelo O. H. et al., 2013, A&A, 560, A29
Shivvers I., Groh J. H., Mauerhan J. C., Fox O. D., Leonard D. C., Filippenko A. V., 2015, ApJ, 806, 213
Smartt S. J., 2015, Publ. Astron. Soc. Aust., 32, e016
Smartt S. J., Maund J. R., Hendry M. A., Tout C. A., Gilmore G. F., Mattila S., Benn C. R., 2004, Science, 303, 499
Smartt S. J., Eldridge J. J., Crockett R. M., Maund J. R., 2009, MNRAS, 395, 1409
Tabernero H. M., Dorda R., Negueruela I., González-Fernández C., 2018, MNRAS, 476, 3106
Utrobin V. P., Chugai N. N., 2005, A&A, 441, 271
Utrobin V. P., Chugai N. N., 2017, MNRAS, 472, 5004
Valenti S. et al., 2016, MNRAS, 459, 3939
Yaron O. et al., 2017, Nat. Phys., 13, 510

This paper has been typeset from a TEX/LATEX file prepared by the author.